Bryant, R.N., et al., 2023, Inorganic sulfate–based signatures of chemosymbiosis in modern infaunal lucinids: Geology, https://doi.org/10.1130/G51353.1

Supplemental Material

Materials and methods, continued.

Figures S1–S4.

Table S1.

SUPPLEMENTAL MATERIALS

Materials and Methods continued

Isotopic notation

We use delta notation to describe the deviation in per mil (‰) of the isotopic composition of samples from known reference standards (Coplen, 2011). For sulfur isotopes, $\delta^{3x}S_{sample} = [(^{3x}S/^{32}S)_{sample}/(^{3x}S/^{32}S)_{V\text{-}CDT}] - 1$, where V-CDT is the Vienna Canyon Diablo Troilite reference standard (Ding et al., 1999). For mass independence calculations, $\Delta^{33}S = \delta`^{33}S\text{-}0.515*\delta`^{34}S$, where $\delta`^{3x}S = 1000\ln[(^{3x}S/^{32}S)_{sample}/(^{3x}S/^{32}S)_{V\text{-}CDT}]$.

Samples

Bathymodiolus azoricus shells were sampled during the MOMARDREAM-NAUT cruise in 2007 in the Mid-Atlantic Ridge (40.06667°, -29.68333°). Tropical shallow-water species were collected in Guadeloupe in low-sulfide seagrass beds of *Thalassia testudinum* (16.21472°, -61.53472°) for the lucinids *Codakia orbicularis* and *Ctena imbricatula* and in a sulfide-rich site of mangrove (16.27583°, -61.55472°) previously investigated to characterize the sediment chemistry (Crémière et al., 2017; Gontharet et al., 2017) for the lucinid *Phacoides pectinatus* and for the non-symbiotic oyster *Crassostrea rhizophor*a attached to the roots of the mangrove trees *Rhizophora mangle* (Supplemental Figure 1A). Locations of sub-sampling for each specimen are shown in Supplemental Figure 1B.

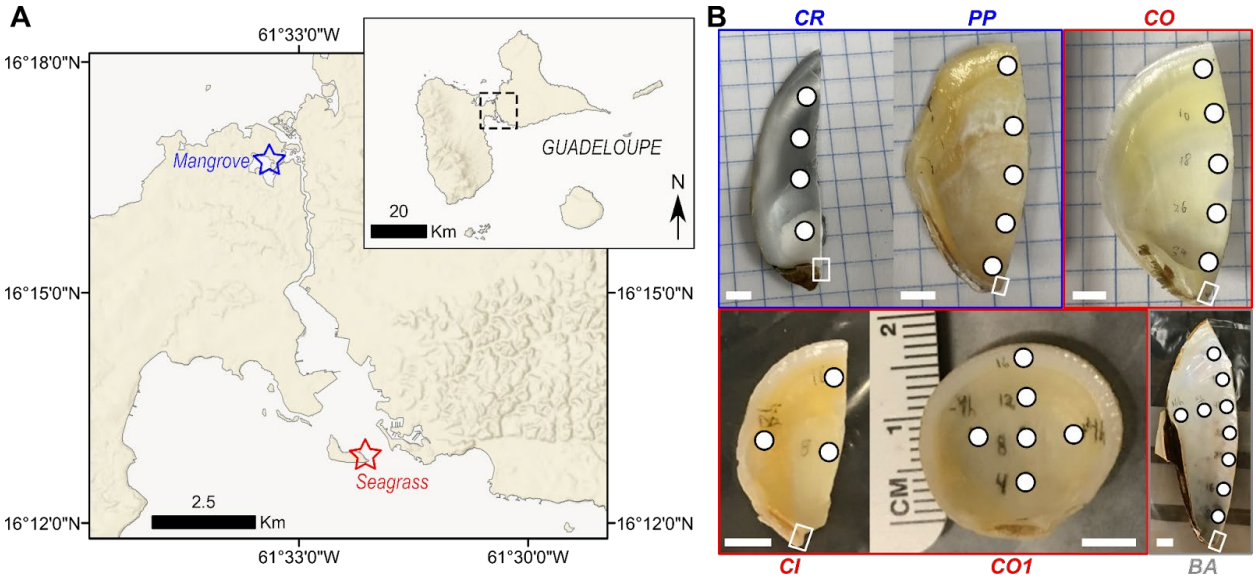

Supplemental Figure 1. Sampling locations. A) Map with stars showing the mangrove and seagrass locations where specimens were collected; dashed rectangle on inset map shows the location of the blown-up map area in Guadeloupe. B) Photos of all specimen shells prior to sub-sampling. Circles show sub-sampling locations; empty white rectangles indicate locations targeted for synchrotron mapping of shell cross sections. Scale bars are all 5mm. Blue-outlined samples are those from the mangrove sediments, red-outlined samples are from the seagrass sediments, and the gray-outlined sample is from the hydrothermal vent.

Carbonate-associated sulfate (CAS) isolation and quantification

CAS was extracted from carbonate samples, quantified, and analyzed for $\delta^{34}S$ using methods slightly adapted from a well-established existing method (Paris et al., 2013, 2014). After sub-sampling with a dental drill, powders were ground with a mortar and pestle for 30 seconds and passed through a 63 µm sieve to standardize the grain size. Powdered carbonate samples (3-5 mg) were then treated with 10% (w/w) NaCl solution in an ultrasonic bath for 18 hours to remove any soluble salts. After rinsing 3 times with ultrapure water, samples were treated with a

5% (vol/vol) NaOCl solution for 48 hours to remove any organic matter-bound sulfur compounds. After rinsing 3 further times with ultrapure water, samples were rinsed with methanol to remove any residual NaOCl and evaporated to dryness. Comparison of pre- and post-bleaching sample mass indicated that an average of ~4% of initial sample material was lost during the bleach treatment. Samples were treated with 5 mL of a 0.1 M acetic acid, 0.05 M ammonium hydroxide solution in an ultrasonic bath for 4-16 hours to ensure complete dissolution of carbonate materials. Each sample was evaporated to dryness at 160°C and run up in 800 µL 3.3 mN HCl. Samples were loaded onto 15 mL Biorad PolyPrep columns packed with 800 µL AG1-X8 anion exchange resin and allowed to equilibrate for 30 minutes. Cations were eluted from columns using 3 rounds of 800 µL ultrapure water and discarded. Anions were eluted from columns using 4 rounds of 800 µL 0.5 N HNO_3 and collected in Teflon vials. The anion fractions were evaporated to dryness at 160°C and run up in 4 mL ultrapure water. A 500 µL aliquot was taken for anion quantification on a Thermo/Dionex ion chromatography system and the remaining 3.5 mL were evaporated to dryness overnight at 100°C to be used for sulfur isotope analysis. For each sample, 200 µL was injected into an Dionex IonPac AS19 column and anions were eluted using ~16 mL 20 mM NaOH. Sulfate was quantified by comparing chromatogram peak areas against a four-point concentration calibration between 5 ppb and 5 ppm sulfur.

Neptune (MC-ICP-MS) methods

The remaining mass of sulfur in the Teflon vials was calculated, allowing all samples to be run up to ~50-100 ppb S (in 2% HNO_3) for mass spectrometry. Contrary to Paris et al. (2013), we used calcium rather than sodium as a dopant responsible for increasing the ionization efficiency of sulfur. Like Paris et al. (2013), we found that a dopant:sulfur ratio >2 limited variability in

instrumental mass fractionation (SI Fig. 2A) and maximized ionization efficiency (SI Fig. 2B) (~100 V signal on ^{32}S per ppm S in medium resolution mode, ~40 V signal per ppm S in high resolution mode). We therefore chose to run all samples at 200 ppb Ca. All samples were run up to a volume of 2 mL and – to account for evaporation – Ca and S were under-concentrated by a fraction consistent with their position in the run. An Apex-Ω desolvating nebulizer (ESI) was used as the sample introduction system, allowing the Neptune to be run in dry-plasma conditions. Sample analyses (roughly 5 minutes in duration) were bracketed by analyses of 100 ppb S, 200 ppb Ca high-purity ICP-MS standard, and all samples and bracketing standards were further bracketed by analyses of 200 ppb Ca high-purity ICP-MS standard (i.e., machine blank). Each run consists of 5 standards of known isotopic composition (2 seawaters, San Salvador aragonite sand, NBS-127 and IAEA-SO-5), 22 samples, and 3 procedural blanks, each of which is run twice and averaged. Runs last for ~24 hours. The machine blanks are simply subtracted from adjacent analyses, and the procedural blanks are subtracted from all sample/standard analyses, accounting for the differential dilution of each sample versus the procedural blanks. The bracketing standards are used as denominators for raw isotopic ratio calculations, accounting for any mid-run instrumental mass fractionation drift. Raw isotopic ratios are then converted to per mil deviations from the VCDT reference standard using the average composition of seawaters in each run. The measured $\delta^{34}S$ values of the other standards are used to verify the accuracy of standardization procedure for each run. The degree of mass independence is also assessed for each sample and standard by calculating $\Delta^{33}S$; standards/samples with $\Delta^{33}S$ more than 0.2 per mil away from zero are discarded.

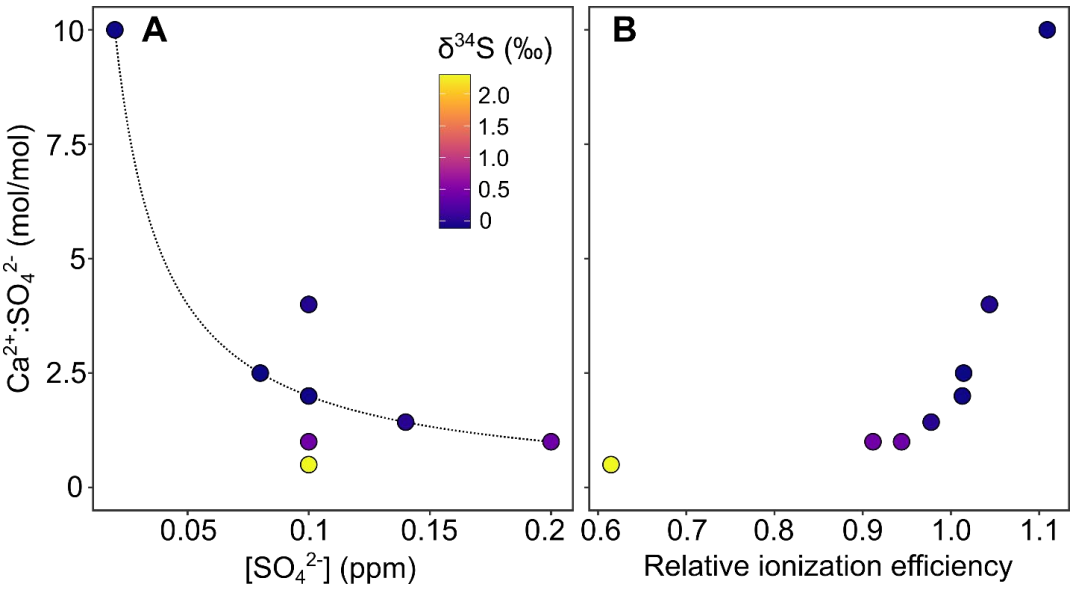

Supplemental Figure 2. Effect of calcium addition on, A) instrumental mass fractionation of sulfur, and B) relative ionization efficiency of sulfur, for mixed sulfur-calcium solutions bracketed by a 100 ppb S, 200 ppb Ca standard. Isotopic data ($\delta^{34}S$ values) are reported relative to the bracketing standard, and relative ionization efficiency is the ratio of the intensity of the sample against the average intensity of the closest bracketing standards, normalized by sulfate concentration. All data are background and drift corrected. The dashed line in panel A represents a constant amount of Ca^{2+} (200 ppb) equivalent to that used for all measurements in this study, showing that the measured ratio is constant if the amount of Ca is twice the amount of sulfate. Panel B shows that a Ca^{2+}:SO_4^{2-} ratio of >2 ensures a high relative ionization efficiency.

Synchrotron methods

Sulfur K-edge micro-X-ray Fluorescence (u-XRF) imaging and X-ray Absorption Near Edge Structure (XANES) spectroscopy was performed at beamline 14-3 at the Stanford Synchrotron Radiation Lightsource (SSRL), SLAC National Accelerator Laboratory, under standard ring conditions of 500 mA and 3 GeV. At BL 14-3 a water cooled double Si (111) monochromator

was used to calibrate the beamline to the S K-edge using the top of the first pre-edge peak of a sodium thiosulfate powder at 2472.02 eV. The X-ray beam was focused to a 5 um spot size using sigray achromatic paraboidal lenses. Measurements were performed at room temperature in a He atmosphere. Multi-energy (ME) μ-XRF imaging combined with XANES spectroscopy is a tool to spatially map the distribution of chemical species of an element within a sample [e.g., (Farfan et al., 2018)]. Energies for mapping were chosen based on the white line position for known S species, and on preliminary XANES spectra, which were 2471.3, 2472.8, 2473.2, 2475.8, 2481.0 and 2482.1 eV. A principal component and simplex volume maximization analysis on the raw multi-energy maps (using the MicroAnalysis toolkit) provided spot locations for XANES spectroscopy. Maps were collected on the cross-sectional area closest to the umbo due to the variability in size and shape of the shells for a more standardized comparison.

Post-processing of data was performed in the MicroAnalysis toolkit (Webb, 2010), SixPACK (Webb, 2005), and Athena (Ravel and Newville, 2005). Repeat XANES spectra were averaged, background subtracted by regressing a line function to the pre-edge and normalized by fitting a second order polynomial to the post-edge region. A PCA of the XANES spectra in SixPACK identified the experimental spectra that are the most dissimilar to one another, and a linear combination fitting of standard spectra to the end-member XANES was used to determine the S species present (unless the XANES spectrum was a single species that could be readily fingerprinted). End-member, single species, XANES spectra were applied to the ME maps using a least-squares fitting to generate a new set of maps that correspond to S species instead of energies.

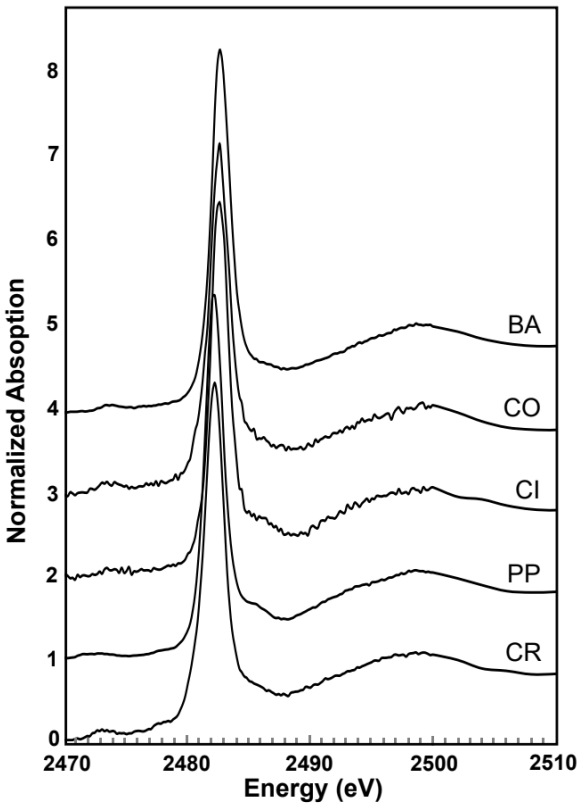

Supplemental Figure 3. Representative S K-edge XANES spectra showing a clear sulfate peak from each clam species. XANES spectra are offset for clarity. Note that the energy position of the sulfate excitation peak in O-CR and L-PP is 2482.2 eV, which is shifted to 2482.6 eV in L-CI, L-L-CO and M-BA. This is most likely a result of differential trace element incorporation (Barkan et al., 2020).

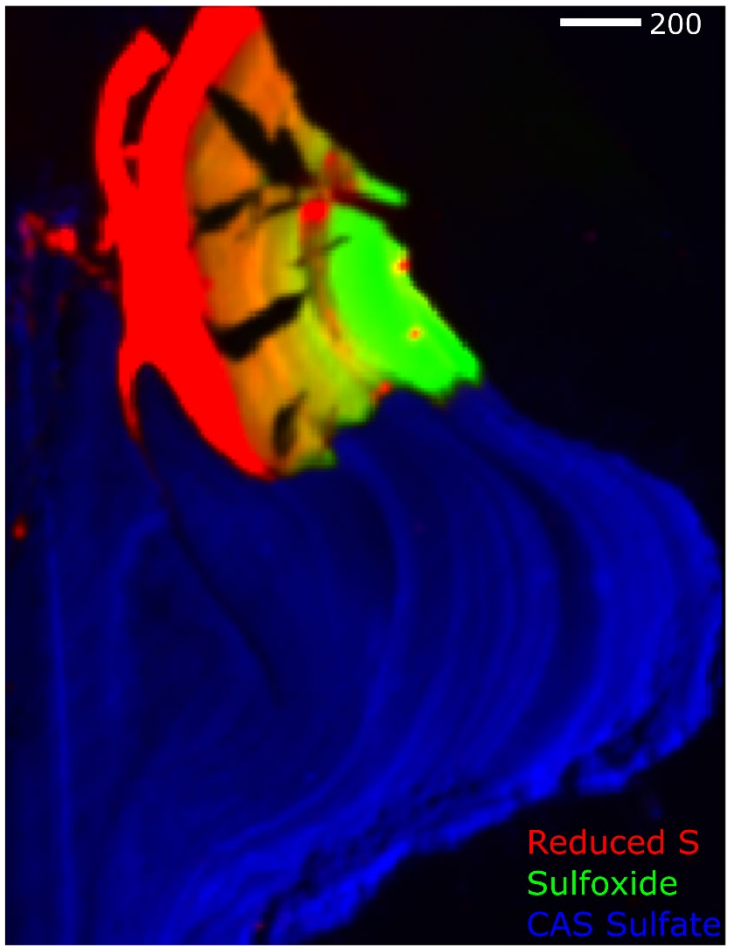

Supplemental Figure 4. S speciation maps of L-PP shell. Tricolor map of reduced S (red), sulfoxide (green), and CAS (blue). Organic S species are scaled to 10x CAS due to the high abundance of organic S moieties in the hinge. A majority of the S in the calcite shell is inorganic sulfate as CAS. Although an intracrystalline organic matrix may be present, the abundance of S in that organic matrix is below the XRF detection limit (<1 ppm). Similar observations are made in all clam species studied herein, as well as in modern carbonate-shelled brachiopods (Richardson et al., 2019). Scale bar is 200 micrometers.

Supplemental Table 1

Sample	Specimen	Normalized distance from umbo	Distance from umbo (mm)	Sample wt. (mg)	CAS (ppm)	Mean± st.dev	δ^{34}S-CAS (‰, VCDT)	Mean± st.dev
CO-2	L-CO	0.95	38	6.4	86	133±49	14.5	15.3± 1.1
CO-10	L-CO	0.75	30	3.69	144		14.4	
CO-18	L-CO	0.55	22	4.3	211		14.7	
CO-26	L-CO	0.35	14	3.08	104		16.4	
CO-34	L-CO	0.15	6	3.26	118		16.6	
PP-2	L-PP	0.94	34	4.28	305	371±47	18.5	18.5± 0.5
PP-10	L-PP	0.72	26	4.75	344		18.8	
PP-18	L-PP	0.50	18	5.12	388		18.9	
PP-26	L-PP	0.28	10	4.9	426		17.7	
PP-34	L-PP	0.06	2	3.13	392		18.4	
CR-2	O-CR	0.96	44	3.77	1187	1076±121	20.9	20.8± 0.2
CR-10	O-CR	0.78	36	3.79	1123		20.8	
CR-18	O-CR	0.61	28	2.43	962		20.7	
CR-26	O-CR	0.43	20	1.81	930		20.6	
CR-34	O-CR	0.26	12	4.21	1175		21.2	
CI-8	L-CI	0.40	8	5.01	25	21±9	13.79	13.8± 1.7
CI-16	L-CI	0.80	16	4.73	26		15.48	
CI-8h	L-CI	0.55	11	4.69	11		12.15	
BA-8	M-BA	0.13	8	4.67	348	193±137	21.87	21.0± 1.0
BA-16	M-BA	0.25	16	5.09	421		21.63	
BA-24	M-BA	0.38	24	4.75	332		22	
BA-32	M-BA	0.50	32	4.79	174		21.64	
BA-40	M-BA	0.63	40	4.94	85		20.04	
BA-48	M-BA	0.75	48	5.01	48		20.36	
BA-54	M-BA	0.84	54	5.13	89		18.99	
BA-8h	M-BA	0.64	41	4.79	116		20.86	

BA-16h	M-BA	0.67	43	4.77	125		21.31	
CO#1-4	L-CO_1	0.22	4	4.91	23	13±6	9.53	9.2± 3.0
CO#1-8	L-CO_1	0.44	8	4.45	17		7.35	
CO#1-12	L-CO_1	0.67	12	4.79	6		5.18	
CO#1-16	L-CO_1	0.89	16	4.47	10		12.94	
CO#1- -4h	L-CO_1	0.72	13	5.68	11		12.21	
CO#1- +4h	L-CO_1	0.72	13	5.56	8		8.12	

REFERENCES

Barkan, Y., Paris, G., Webb, S.M., Adkins, J.F., and Halevy, I., 2020, Sulfur isotope fractionation between aqueous and carbonate-associated sulfate in abiotic calcite and aragonite: Geochimica et Cosmochimica Acta, v. 280, p. 317–339, doi:10.1016/j.gca.2020.03.022.

Coplen, T.B., 2011, Guidelines and recommended terms for expression of stable-isotope-ratio and gas-ratio measurement results: Rapid Communications in Mass Spectrometry, v. 25, p. 2538–2560, doi:10.1002/rcm.5129.

Crémière, A., Strauss, H., Sebilo, M., Hong, W.L., Gros, O., Schmidt, S., Tocny, J., Henry, F., Gontharet, S., and Laverman, A.M., 2017, Sulfur diagenesis under rapid accumulation of organic-rich sediments in a marine mangrove from Guadeloupe (French West Indies): Chemical Geology, v. 454, p. 67–79, doi:10.1016/j.chemgeo.2017.02.017.

Ding, T., Bai, R., Li, Y., Wan, D., Zou, X., and Zhang, Q., 1999, Determination of the absolute32S/34S ratio of IAEA-S-1 reference material and V-CDT sulfur isotope standard: Science in China Series D: Earth Sciences, v. 42, p. 45–51, doi:10.1007/BF02878497.

Farfan, G.A., Apprill, A., Webb, S.M., and Hansel, C.M., 2018, Coupled X-ray Fluorescence and X-ray Absorption Spectroscopy for Microscale Imaging and Identification of Sulfur Species within Tissues and Skeletons of Scleractinian Corals: Analytical Chemistry, v. 90, p. 12559–12566, doi:10.1021/acs.analchem.8b02638.

Gontharet, S., Crémière, A., Blanc-Valleron, M.M., Sebilo, M., Gros, O., Laverman, A.M., and Dessailly, D., 2017, Sediment characteristics and microbial mats in a marine mangrove, Manche-à-eau lagoon (Guadeloupe): Journal of Soils and Sediments, v. 17, p. 1999–2010, doi:10.1007/s11368-016-1555-6.

Paris, G., Adkins, J.F., Sessions, A.L., Webb, S.M., and Fischer, W.W., 2014, Neoarchean carbonate-associated sulfate records positive $\Delta^{33}S$ anomalies.: Science (New York, N.Y.), v. 346, p. 739–41, doi:10.1126/science.1258211.

Paris, G., Sessions, A.L., Subhas, A. V., and Adkins, J.F., 2013, MC-ICP-MS measurement of δ34S and Δ33S in small amounts of dissolved sulfate: Chemical Geology, v. 345, p. 50–61, doi:10.1016/j.chemgeo.2013.02.022.

Ravel, B., and Newville, M., 2005, ATHENA, ARTEMIS, HEPHAESTUS: Data analysis for X-ray absorption spectroscopy using IFEFFIT, *in* Journal of Synchrotron Radiation, International Union of Crystallography, v. 12, p. 537–541, doi:10.1107/S0909049505012719.

Richardson, J.A., Newville, M., Lanzirotti, A., Webb, S.M., Rose, C. V., Catalano, J.G., and Fike, D.A., 2019, The source of sulfate in brachiopod calcite: Insights from μ-XRF imaging and XANES spectroscopy: Chemical Geology, v. 529, p. 119328, doi:10.1016/j.chemgeo.2019.119328.

Webb, S.M., 2005, SIXpack: A graphical user interface for XAS analysis using IFEFFIT: Physica Scripta T, v. T115, p. 1011–1014, doi:10.1238/Physica.Topical.115a01011.

Webb, S.M., 2010, The microAnalysis toolkit: X-ray fluorescence image processing software, *in* AIP Conference Proceedings, v. 1365, p. 196–199, doi:10.1063/1.3625338.